Journal of Physics: Condensed Matter

LETTER

Polariton condensate trapping by parametric pair scattering

To cite this article: G G Paschos *et al* 2020 *J. Phys.: Condens. Matter* **32** 36LT02

IOP Publishing Journal of Physics: Condensed Matter
J. Phys.: Condens. Matter **32** (2020) 36LT02 (6pp) https://doi.org/10.1088/1361-648X/ab9267

Letter

Polariton condensate trapping by parametric pair scattering

G G Paschos[1,2,3], A Tzimis[3], S I Tsintzos[3,4] and P G Savvidis[1,2,3,5,6]

[1] Westlake University, 18 Shilongshan Rd, Hangzhou 310024, Zhejiang, People's Republic of China
[2] Westlake Inst Adv Study, National Institute of Sciences, 18 Shilongshan Rd, Hangzhou 310024, Zhejiang, People's Republic of China
[3] Foundation for Research and Technology-Hellas, Institute of Electronic Structure and Laser, 71110 Heraklion, Crete, Greece
[4] Eulambia Advanced Technologies Ltd., Ag. Ioannou 24, 15342, Athens, Greece
[5] Department of Nanophotonics and Metamaterials, ITMO University, 197101 St. Petersburg, Russia

E-mail: p.savvidis@westlake.edu.cn

Received 18 February 2020, revised 30 April 2020
Accepted for publication 12 May 2020
Published 17 June 2020

Abstract

Spatially confined, trapped polariton condensates have been shown to exhibit strong stochastic on-site spin polarization and in longer polariton condensate chains, distance controlled ferromagnetic and antiferromagnetic spin couplings. Until now, little is known, on how such polariton condensates spatially separated from their exciton reservoirs are trapped and formed. Here, we investigate the properties and formation dynamics of two main families of polariton condensates, those overlapping with the pump reservoir and those in confined geometries, under pulsed nonresonant excitation. The observed reduction in polariton condensation threshold and energy blueshift in trapped case is attributed to exciton reservoir-condensate spatial separation, whereas time-resolved photoluminescence measurements, reveal distinct relaxation and condensate formation dynamics with pair parametric scattering process being the dominant relaxation mechanism in trapped geometry.

Keywords: polariton, condensate, time-resolved, blueshift

S Supplementary material for this article is available online

(Some figures may appear in colour only in the online journal)

1. Introduction

Microcavity polaritons can be localized [1] or propagate [2] in real space with respect to the potential landscape created along the plane of motion. Intrinsic disorder of the crystal lattice, patterning on the sample (mesas, wave-guides) [3], application of electromagnetic fields [4, 5], and polariton self-interactions [6, 7], can modify the potential landscape, thus amending the optical properties and relaxation dynamics of polariton condensates.

Polaritons being half-exciton–half-photon quasi-particles, can propagate for hundred of micrometers [8] due to their photonic component, and show strong non-linear interactions through their excitonic component. Their bosonic nature allows them to form coherent condensates [9, 10] which can be easily manipulated by using various pump spot configuration geometries [11–13]. Control of polariton propagation by imprinting optically generated potentials on a semiconductor

[6] Author to whom any correspondence should be addressed.

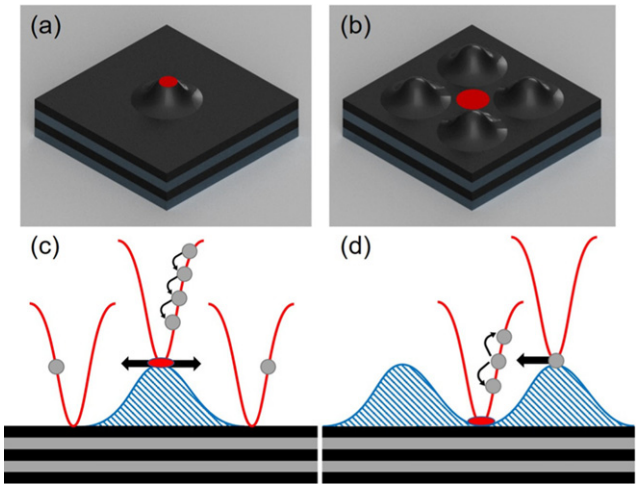

Figure 1. Schematic of the un-trapped condensate with single pump spot (a) trapped condensate with four pump spots (b). Corresponding energy landscapes and position dependent lower polariton branch (LPB) (c) and (d). In the un-trapped case, condensate polaritons forming at the pump are radially ejected by potential gradient (c) whereas in the trapped geometry (d), low energy uncondensed polaritons ejected towards potential minima are trapped by losing energy via parametric pair scattering and form condensate.

microcavity surface enables the shaping of the potential landscape which simultaneously determines the polariton condensate formation mechanism. Condensate lattices of both trapped [14] and freely expanding polariton condensates (un-trapped) have been recently extensively studied in the context of using such systems for analog quantum simulation [15–18]. The former showing peculiar transition from synchronized superfluid state to isolated condensate state [11] with the latter realizing classical XY Ising spin Hamiltonian [19]. Even though trapped and un-trapped polariton condensates have been extensively studied, demonstrating high stability [20], polarizability [21] and precise control between neighbour interactions in polariton condensate lattices [22–24], yet until now, no direct comparison of the relaxation and formation dynamics of these two distinct condensation regimes has been performed.

In this study, we employ spatially patterned laser excitation to either generate single narrow beam with the condensate forming at its center or multiple laser beams to produce the trapping potential inside which polariton condensate is formed, as shown in figures 1(a) and (b). We show that by spatially separating polariton condensate from exciton reservoirs on which polaritons strongly scatter, it is possible to decrease lasing threshold, emission linewidth as well as energy blueshift. Furthermore, by performing time and angle-resolved photoluminescence (PL) imaging measurements we elucidate an explicit difference in polariton condensate relaxation and condensate formation dynamics. In the trapped pumping configuration, we observe a new relaxation mechanism via parametric pair scattering process, triggered by the feeding of low energy polaritons from surrounding polaritonic states with well defined in-plane wavevectors [25–27].

2. Materials and methods

The sample under consideration [28] is a high quality factor ($Q \sim 16\,000$) semiconductor microcavity (figures 1(a) and (b)) grown by molecular beam epitaxy (MBE). The $5\lambda/2$ microcavity is sandwiched between two distributed Bragg reflectors (DBRs) constituting of 32 (top) and 35 (bottom) AlAs/AlGaAs pairs, while four sets of three 10 nm $Al_{0.3}Ga_{0.7}As$/GaAs quantum wells (QWs) are located at the maximum of the stationary electric field, thus enhancing light–matter interactions. The sample is placed in a closed-cycle cryostat and cooled down to 7 K.

To spatially modulate the laser beam, we employ a computer controlled spatial light modulator based on digital micromirror device (DMD) technology to generate both excitation schemes on demand, as shown in figure 1. A mixture of bright and dark excitons as well as polaritons is formed from the initially injected electron–hole plasma. Due to considerable diffusion of dark excitons from the initial pump spots, (determined by their long non-radiative lifetime) the smallest FWHM potential energy landscape features resulting from repulsive exciton–exciton interaction [29], which can be imprinted onto the sample are of the order of $\sim$5 μm [30].

In figure 1, the two excitation geometries along with the corresponding energy potential landscapes are presented. One pump spot with a diameter of 8 μm allows the creation of freely expanding un-trapped condensate with polaritons ejected in different direction converting their potential energy into kinetic of well-defined in-plane wavevector, as shown in figures 1(a) and (c). Correspondingly, the use of an excitation pattern of four spots with a diameter of 8 μm each, separated by 12 μm distance, leads to the formation of trapped polariton condensate. In this case, the condensate is formed by energy relaxing low energy polaritons, ejected from the pump spots, which are consequently trapped at the center of four spots at increased pump densities, as shown by the red disk in figures 1(b) and (d). Despite many recent observations of trapped polariton condensates [31–35] demonstrating peculiar spin polarization phenomena in a variety of complex geometries, the precise mechanism of energy relaxation and trapping of polaritons, subject of the present study, has yet to be elucidated in contrast to the single spot case [36–40].

3. Results

3.1. Polariton condensates using one and four pump spot excitation

We study the non-linear properties of polaritons by performing angle-resolved PL imaging and power dependence measurements using pulsed optical excitation tuned at 1.649 eV, with a repetition rate of 87 MHz and pulse width of 150 fs. The sample is excited at the first minimum on the high energy side of the DBR reflection. The PL collected via large NA objective is spatially filtered with a pinhole to ensure that the recorded light arises only from the condensate area and not from the surrounding reservoirs.

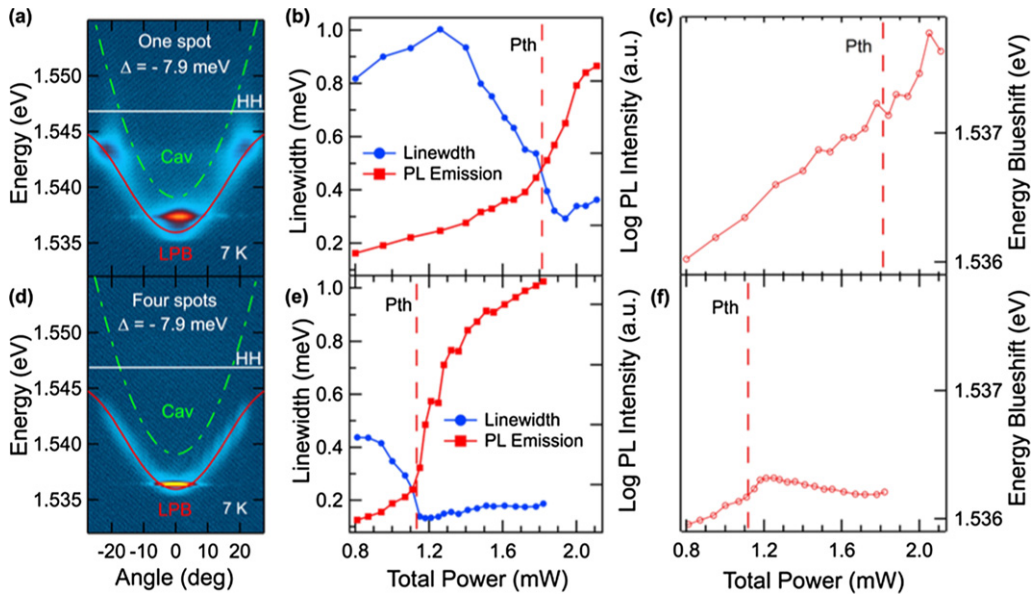

Figure 2. Polariton PL and dispersions at threshold for un-trapped single spot (a) and trapped four spot (d) condensation geometries at 7 K and sample detuning of $\Delta = -7.9$ meV. Integrated normal incidence PL intensity and linewidth with increasing pump power for one (b) and four (e) spot excitation. Corresponding LPB energy shifts (c) and (f).

The recorded PL emission from un-trapped and trapped excitation geometries are plotted in figures 2(a) and (d) respectively together with the corresponding polariton dispersions fits (red lines) obtained using a coupled harmonic oscillator model [28]. The dispersion curves clearly confirm the presence of the strong coupling regime with extracted Rabi splitting of 9.2 meV.

Power dependence experiments for both excitation geometries were performed at the same negative exciton-cavity detuning −7.9 meV for better comparison. In figures 2(b) and (c) the integrated PL intensity as well as the respective emission linewidth with the increasing total excitation power is presented (1 and 4 spots).

Above lasing threshold ($P_{\rm th}$), a non-linear increase of the PL intensity is observed (red squares) together with a simultaneous reduction of the emission linewidth, indicating the formation of the polariton condensate. In figures 2(c) and (f), the extracted from the data polariton condensate energy blueshift as a function of pump power for the two excitation geometries is depicted.

Our results show distinct spectral differences between un-trapped and trapped condensates, related to the geometry of the excitation spots and condensate formation process. For the single spot configuration, at the threshold ($P_{\rm th} = 1.8$ mW), we obtain emission linewidth of 0.4 meV, which broadens at higher excitation power due to spatial overlap of the condensate with increasing exciton reservoir which increases linearly with pump power. Similarly, the condensate energy blueshift, which is determined by the strength of the exciton–polariton interaction and reservoir density, increases linearly as shown in figure 2(c).

We note that the measured condensate linewidths are extracted from a temporal average of the emission starting from the impact of the pulse until the arrival of the next pulse. Therefore, condensate emission linewidth is partially broadened due to time averaging. However, since the induced energy blueshifts are mainly controlled by instantaneously created exciton reservoir densities which decay on a nanosecond time scale, and because condensate emission occurs only within short 50–100 ps time interval from pump arrival, the induced broadening to the condensate emission linewidth is insignificant.

On the contrary, in the four spot excitation geometry, due to the spatial isolation of the trapped condensate from the pump reservoir, we obtain reduced linewidths, blueshift and lasing threshold values. The extracted condensate linewidth of 0.13 meV at threshold is almost half the value obtained in the single spot geometry. In addition, the corresponding energy blueshift 0.3 meV is ∼4 times smaller, since excitons do not diffuse to such long distances, while contribution of onsite polariton–polariton interactions to the blueshift becomes dominant [41].

Furthermore, the lasing threshold appears reduced in the case of the four spot pattern, $P_{\rm th} = 1.16$ mW, in agreement with previous reports by Cristofolini *et al* [42]. Such reduction in the lasing threshold was attributed to collective feeding of the central condensate from surrounding reservoirs, by low energy polaritons ejected from the peaks and being trapped at the potential minima, providing an efficient route to populating the condensate state. On the contrary, in the case of single excitation spot, polaritons are ejected away from the condensate formation area, thus requiring larger pump power to reach the condensation threshold. In the next section, we examine the validity of these assumptions by performing detailed time resolved PL experiments to unveil the mechanism behind the polariton energy relaxation and condensate formation dynamics for both excitation schemes.

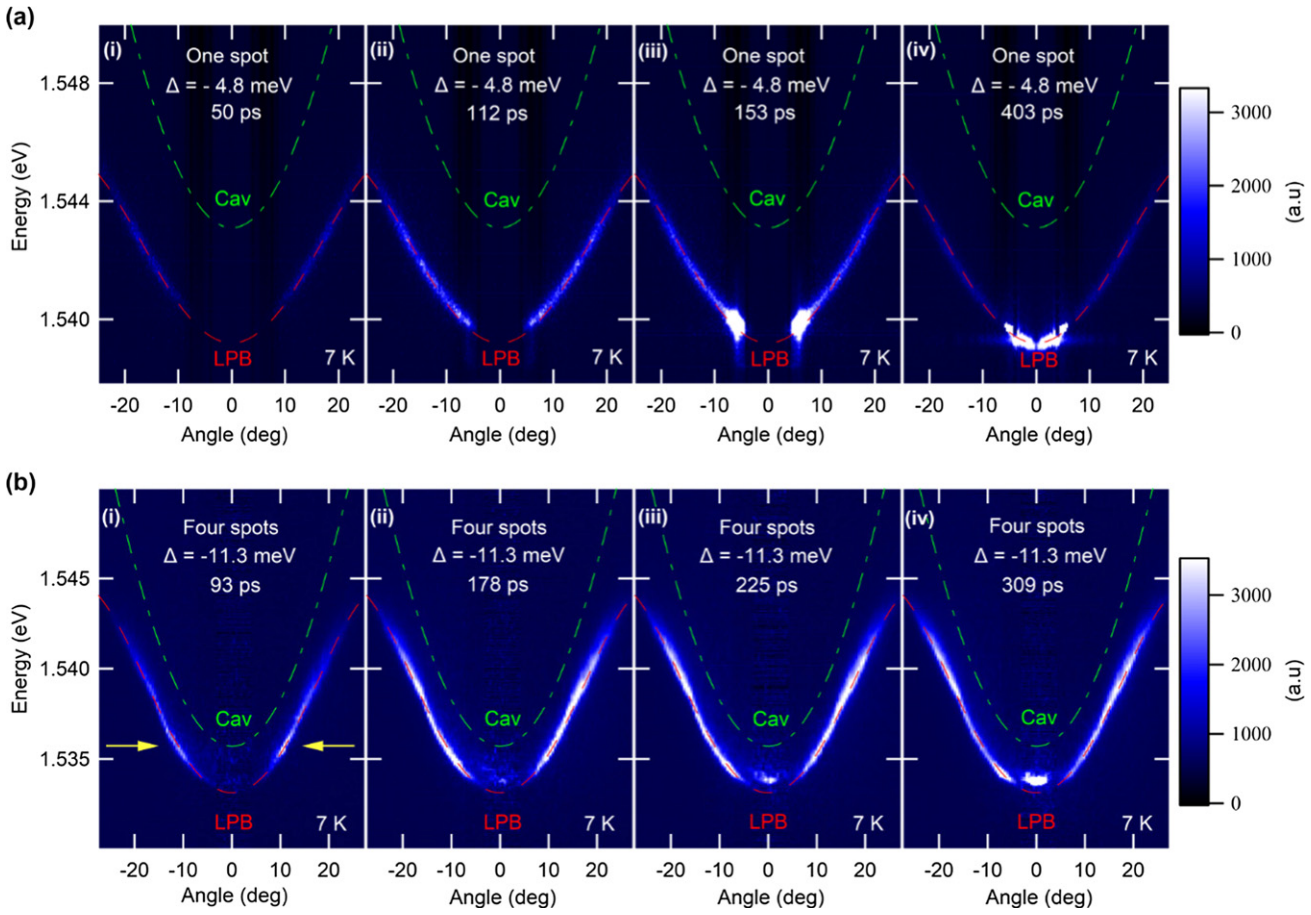

Figure 3. Snapshots of time resolved PL and polariton dispersions for one (a) and four (b) spot excitation. Progressive energy relaxation of polaritons along the LPB (a) (i) and (ii) followed by polariton lasing on either side of the LPB (a) (iii). Relaxation of polaritons to the bottom of the LPB (a) (iv). Injection of polaritons at specific wavevectors from surrounding peaks (yellow arrows) (b) (i). Simultaneous occupation of high and low energy states driven by parametric pair scattering (b) (ii) and initial condensate formation at $k_{//} = 0$ (b) (iii). Parametric scattering continuously feeding and sustaining polariton condensation at larger times (b) (iv).

3.2. Relaxation dynamics of trapped and un-trapped polariton condensates

Energy resolved tomography has been used in earlier studies by Nardin *et al* [43] to map excited states of trapped condensates and employed streak camera to energy resolve real space polariton dynamics [44]. To study polariton energy relaxation dynamics we employ a specially developed *k*-space time domain tomography technique by coupling a streak camera to a spectrometer. This is achieved by collecting angular PL with a large NA objective, whose Fourier (back focal) plane is projected onto the entrance slit of the spectrometer. The spectrometer selects a specific narrow angular range of 0.5 degrees (corresponding to $\Delta k_{//} = 1.35\,\mathrm{cm}^{-1}$ in-plane wavevector range), spectrally resolves it, and couples it onto the horizontal slit of the streak camera to obtain the time evolution of the emission at each energy. The Fourier plane is continuously vertically scanned by an external mirror across the spectrometer slit to selectively couple the whole PL angular range in steps of 0.5 degrees. Once the 3D data are acquired, tomographic slices in time domain reveal carrier relaxation dynamics along the polariton dispersion branches. We note that each streak camera image represents an average over hundreds of thousands of traces following the incidence of the pump pulse.

This tomographic technique enables the investigation of the polariton dynamics for various k states, both in single and four pump spot configurations for an excitation power slightly above the condensation threshold. In figure 3, far-field PL emission images at various times after initial excitation are plotted for the trapped ($\Delta = -4.8$ meV) and un-trapped ($\Delta = -11.3$ meV) condensation geometries. The particular detunings were chosen to yield lowest possible thresholds for both configurations. For clarity, the position of the LPB is shown throughout all images. For single spot geometry, figure 3(a), we excite the sample with an optical power of 1.9 mW ($1.26P_{\mathrm{th}}$). Polaritons initially occupy high k-states and rapidly relax towards the bottom of the LPB forming the un-trapped polariton condensate [seen clearly in movie 1 of supplementary info (https://stacks.iop.org/JPCM/32/36LT02/mmedia)]. At 50 ps (figure 3(a(i))), an initial increase in the PL emission along the LPB dispersion is observed, reflecting the time scale required for the exciton formation and relaxation into radiative polaritonic states. As larger occupancies of the states along the dispersion are reached, PL emission intensity increases dramatically (figure 3(a(ii))), eventually leading to the onset of

polariton lasing seen in figure 3(a(iii)). Notably, the intense PL emission at 1.539 eV, either side of the LPB branch, indicates that condensate polaritons are ejected radially, acquiring well-defined in plane momentum from the local potential maxima formed by repulsively interacting high density exciton reservoir overlapping with the condensate. At later times, once the exciton reservoir decays and diffuses laterally, condensate polaritons are no longer ejected as seen in figure 3(a(iv)) where PL emission arises from the bottom of the LPB.

For the four spot pumping scheme, no condensation and relaxation is expected to occur at early times in the trapped region. Therefore, to observe polariton relaxation and condensate formation, it is important to include in the observation area the four pump spots where the PL initially builds-up. Furthermore, by taking a vertical slice in k-space only the movement of polaritons along the vertical axis is recorded. In figures 3(b(i)–(iv)), several snapshots of the polariton dispersions are recorded at different times when MC sample is excited by four pump beams with a total power of 1.35 mW ($1.28P_{\mathrm{th}}$). It reveals a completely different polariton relaxation process towards the zero k-state of the LPB clearly seen in the movie 2. In contrast to the single spot excitation scheme the created four exciton reservoirs do not spatially overlap with the condensate. Low energy polaritons, created at the pump spots before their condensation, feed the local minima of potential energy at the centre injecting polaritons (yellow arrows figure 3(b(i))) several meV above the LPB ground state and producing distinct emission lobes at an angle of ∼12 degrees. At later times, each lobe in the emission splits into two separate peaks. One peak shifts to lower energies and eventually occupies the ground state at around 178 ps (figure 3(b(ii))), while the other moves higher in energy. As polaritons relax to lower states parametric scattering further assists the relaxation until the onset of condensate in the ground state at ∼225 ps as seen in figure 3(b(iii)). The appearance of signal and idler PL peaks along the polariton dispersion, clearly seen in the figure 3(b(iv)) is a strong indication that under this excitation geometry the parametric scattering of polaritons is responsible for the observed relaxation mechanism.

To further confirm this hypothesis, we extract the angle integrated PL emission spectra versus time for the two pump geometries presented in figures 4(a) and (c). Such emission spectra provide clear picture for polariton relaxation and occupancies along the LPB with time. For the single pump spot excitation, the extracted in figure 4(b) emission peak positions show continuous shift to lower energy states indicative of polariton relaxation along LPB via exciton–polariton scattering. This scattering process, which controls the relaxation process strongly depends on the reservoir exciton density and the spatial overlap between the polariton condensate and the reservoir leading to the faster depletion of the exciton reservoir. Around 150 ps, figure 4(a), PL emission spectrally narrows and increases non-linearly indicating the onset of polariton lasing (figure 4(b), grey area) arising from the un-trapped condensate. This picture is dramatically different in the four pump spot geometry. Here, the strongly suppressed overlap

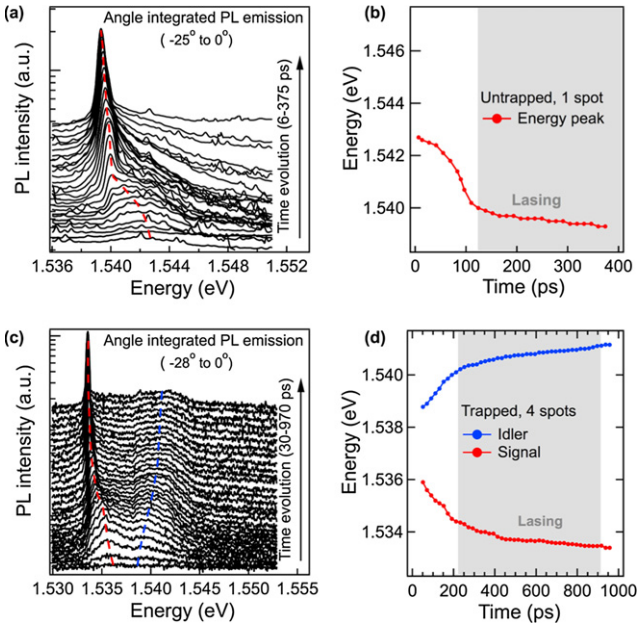

Figure 4. Time resolved angle-integrated PL emission (between −25 and 0 deg) using one (a), (b) and four (c), (d) spot excitation (−28 and 0 deg) showing energy relaxation of polaritons. Single extracted peak emission position showing continuous relaxation of polaritons to low energy states (b). Two peaks corresponding to signal and idler emission peaks is a clear signature of parametric relaxation of polaritons along the LPB (c) and (d).

between polariton condensate and exciton reservoir, leads to suppression of the main exciton–polariton scattering mechanism responsible for condensation. Therefore, other mechanisms are required to populate the trapped states from far apart. As seen in figure 4(d), two distinct emission peaks shown by the red and blue lines corresponding to the scattered signal and idler polaritons with identical energy shifts manifest a clear signature of parametric pair scattering process. Similarly, once sufficient polariton density accumulates in the ground state the onset of lasing emission is observed at around 225 ps, marked by grey area. The different timescales for the onset of condensation are attributed to the longer times required for the relaxation and ejection processes to occur in systems with large spatial separation between exciton reservoir and condensate. Furthermore, slow depletion rates of exciton reservoir due to small overlap between condensate and reservoir allow for the system to decay on much longer timescales in contrast to single spot case when strong overlap leads to rapid depletion and decay of the condensate emission. Finally, our observations highlight the role of parametric pair scattering process as the dominant relaxation mechanism enabling condensation in an area of the sample with very low exciton reservoir densities.

4. Conclusions

In conclusion, we performed a detailed study of polariton relaxation dynamics in two different pump geometries yielding trapped and un-trapped polariton condensates. Our experiments reveal new relaxation mechanism by pair parametric scattering process and shed new light on the condensate

formation dynamics in these two distinct excitation regimes. Since both of these condensation schemes have been utilized to generate polariton condensates lattices for their use in analog polaritonic quantum simulators, understanding their differences and advantages will be vital for the future progress.

Acknowledgments

This research is co-financed by Greece and the European Union (European Social Fund—ESF) through the Operational Programme 'Human Resources Development, Education and Lifelong Learning 2014–2020' in the context of the project 'Analog Polariton Simulator' (MIS 5004464). P S acknowledges financial support from the Westlake University Foundation and the program 2018R01002 supported by Leading Innovative and Entrepreneur Team Introduction Program of Zhejiang. The authors acknowledge Russian Science Foundation Grant No. 19-72-20120 for financial support.

ORCID iDs

G G Paschos https://orcid.org/0000-0001-9762-6971
P G Savvidis https://orcid.org/0000-0002-8186-6679

References

[1] Cristofolini P *et al* 2013 *Phys. Rev. Lett.* **110** 186403
[2] Wertz E *et al* 2008 *Nat. Phys.* **6** 860–4
[3] Paschos G G *et al* 2018 *Sci. Rep.* **8** 10092
[4] Tsotsis P *et al* 2014 *Appl. Phys. Rev.* **2** 014002
[5] Tsintzos S I *et al* 2018 *Phys. Rev. Lett.* **121** 037401
[6] Daskalakis K S *et al* 2014 *Nat. Mater.* **13** 271–8
[7] Ferrier L *et al* 2011 *Phys. Rev. Lett.* **106** 126401
[8] Gao T *et al* 2012 *Phys. Rev.* B **85** 235102
[9] Kasprzak J *et al* 2006 *Nat. Phys.* **443** 409–14
[10] Balili R *et al* 2007 *Science* **316** 1007–10
[11] Ohadi H *et al* 2018 *Phys. Rev.* B **97** 195109
[12] Askitopoulos A *et al* 2015 *Phys. Rev.* B **92** 035305
[13] Dreismann A *et al* 2014 *Proc. Natl Acad. Sci. USA* **111** 8770
[14] Ohadi H *et al* 2015 *Phys. Rev.* X **5** 031002
[15] Amo A and Bloch J 2016 *Compt. Rendus Phys.* **17** 934–45
[16] Angelakis D G 2017 *Quantum Simulations with Photons and Polaritons* (Cham: Springer) DOI: https://doi.org/10.1007/978-3-319-52025-4
[17] Ghosh S and Liew T C H 2020 *npj Quantum Inf.* **6** 16
[18] Lagoudakis P G and Berloff N G 2017 *New J. Phys.* **19** 125008
[19] Berloff N G *et al* 2017 *Nat. Mater.* **16** 1120–6
[20] Deng H, Haug H and Yamamoto Y 2010 *Rev. Mod. Phys.* **82** 1489–537
[21] Ohadi H *et al* 2016 *Phys. Rev. Lett.* **116** 106403
[22] Ohadi H *et al* 2017 *Phys. Rev. Lett.* **119** 067401
[23] Alyatkin S *et al* 2019 arXiv:1907.08580v1
[24] Kalinin K P and Berloff N G 2020 *Adv. Quantum Technol.* **3** 1900065
[25] Savvidis P G *et al* 2000 *Phys. Rev. Lett.* **84** 1547–50
[26] Savvidis P G *et al* 2000 *Phys. Rev.* B **62** R13278
[27] Kundermann S *et al* 2003 *Phys. Rev. Lett.* **91** 107402
[28] Tsotsis P *et al* 2012 *New J. Phys.* **14** 023060
[29] Paschos G G *et al* 2017 *Sci. Rep.* **7** 11377
[30] Anton C *et al* 2012 *Appl. Phys. Lett.* **101** 261116
[31] Harrison S L *et al* 2020 *Phys. Rev.* B **101** 155402
[32] Pieczarka M *et al* 2020 *Nat. Commun.* **11** 429
[33] Ballarini D *et al* 2019 arXiv:1911.02923
[34] Alyatkin S *et al* 2019 arXiv:1907.08580v1
[35] Sun Y *et al* 2017 *Nat. Phys.* **13** 870–5
[36] Wouters M 2008 *Phys. Rev.* B **77** 115340
[37] Wouters M 2010 *Phys. Rev.* B **82** 245315
[38] Tassone F and Yamamoto Y 1999 *Phys. Rev.* B **59** 10830
[39] Porras D *et al* 2002 *Phys. Rev.* B **66** 085304
[40] Ciuti C *et al* 2003 *Semicond. Sci. Technol.* **18** S279
[41] Love A P D *et al* 2008 *Phys. Rev. Lett.* **101** 067404
[42] Cristofolini P *et al* 2013 *Phys. Rev. Lett.* **110** 1864
[43] Nardin G *et al* 2010 *Superlattices Microstruct.* **47** 207–12
[44] Christmann G *et al* 2014 *New J. Phys.* **16** 103039